Rayleigh–Bénard type PCM melting and solid drops

Rayleigh–Bénard type PCM melting and solid drops

Claudia Naldi[1], Giulia Martino[1], Matteo Dongellini[1], Sylvie Lorente[2*]
1 Department of Industrial Engineering
University of Bologna, Viale del Risorgimento 2, 40136 Bologna, Italy
2 Mechanical Engineering Department
Villanova University, 800 Lancaster Ave., Villanova, PA 19085, USA

Abstract

In this paper we document both theoretically and numerically the melting of PCM in an enclosure heated from the bottom, in the presence of vertical metallic fins. We start with the analysis of the PCM melting in the absence of fins to discover the main scales of the problem, stressing the occurrence of Rayleigh-Bénard cells generated during the convection regime of melting. We continue with predicting the impact of fins on the development of the melting interface. The numerical experiments allow to understand the impact of the aspect ratio between the height of the enclosure and the distance between fins on the melting dynamics. They highlight the existence of solid drops for a certain range of aspect ratios when the horizontal flow channels in the convective loops along the fins become in contact, and they show how the solid drop is dragged downward to finish melting on the heated bottom of the enclosure.

Keywords: Phase Change Materials, theoretical and numerical analysis, melting, bottom heated cavity, fins.

[*] Corresponding author: sylvie.lorente@villanova.edu

Nomenclature

c_p	Specific heat capacity at constant pressure, J/(kg·K)
c_p^*	Modified specific heat capacity at constant pressure, J/(kg·K)
Fo	Fourier number
g	Gravitational acceleration, m/s^2
H	Vertical dimension of the enclosure, m
h	Fin height, m
k	Thermal conductivity, W/(m·K)
L	Horizontal dimension of the enclosure, m
l	Fin spacing, m
L_f	Latent heat of fusion, J/kg
Nu	Nusselt number
p	Pressure, Pa
Pr	Prandtl number
q″	Heat flux, W/m^2
Ra	Rayleigh number
Ste	Stefan number
T	Temperature, K
t	Time, s
$\vec{u}$	Velocity vector, m/s
x	Thickness of the boundary layer, m

Greek Letters

α	Thermal diffusivity, m^2/s

β Coefficient of thermal expansion, K^{-1}

δ Melt layer height, m

θ Local liquid fraction

$\bar{\theta}$ Average liquid fraction

μ Dynamic viscosity, Pa s

ν Kinematic viscosity, m^2/s

ρ Density, kg/m^3

Subscripts

* Based on $\Delta T / 2$

f Fins

m Melting

trans Transition between conduction and convection

Abbreviations

PCM Phase Change Material

RMSD Root Mean Square Deviation

1. Introduction

The use of Phase Change Materials (PCMs) allows to store large amounts of heat, both sensible and latent, with a significant increase in the storage capacity thanks to latent heat. Yet, the generally poor thermal conductivity of PCMs limits their ability to be an efficient thermal energy storage solution. This is why the relative allocation of the volume of PCM with regards to the heat source is of paramount importance as demonstrated in [1] and [2] through scale analysis and numerical experiments. As a result, several studies have been carried out in the last years to

improve the heat transfer within PCMs, either enhancing the convective heat transfer [3]-[7], or adding high conductivity components like nanoparticles [8]-[10], metal foams [11]-[14], or metal fins [15]-[19].

In order to study the influence of natural convection on the PCM melting and solidification processes in bottom-heated configurations, different research works have been conducted. Parsazadeh and Duan [3] analyzed, both numerically and experimentally, the melting process of coconut oil in the presence of Rayleigh–Bénard cells. In particular, a rectangular enclosure filled with PCM and heated from the bottom was considered. The numerical and experimental results showed that two different regimes occur during the melting process, as functions of the Rayleigh number. While heat conduction is dominant in the first part of the process (low values of the Rayleigh number), when the critical Rayleigh number is overcome, natural convection becomes more efficient, with a consequent change in the shape of the phase change interface from planar to waveform. In addition, Parsazadeh et al. [4] found that the critical Rayleigh number strongly depends on the enclosure size. Several authors studied the melting process of low Pr-number PCMs. In particular, Guo et at. [5] showed that the presence of convective cells causes oscillation of the Nusselt number in the convection-dominated regime, with a consequent reorganization of the flow cells and a distortion of the isothermal lines. Moreover, the melting time decreased considerably going from high to low Pr-number PCMs. Satbhai and Roy [6] numerically studied the buoyancy-driven convection for moderate/fast-melting low Pr-number PCMs in a square box, finding that the onset of convection depends on Stefan and Fourier numbers, in addition to Rayleigh number. Xie and Wu [7] analyzed the PCM melting in a rectangular cavity with different aspect ratios, under the condition of constant heat flux at the left/bottom wall. Their results showed that the

melting time increases with the increase of the cavity aspect ratio, for both left and bottom wall heating conditions.

The effects of the inclusion of metal fins in order to speed up the melting/solidification of PCMs have been widely studied in the literature. Shukla et al. [15] numerically investigated the phase change in a metallic heat exchanger, filled with an organic PCM, with tree-shaped fins. They showed how the PCM melting and solidification time decreases as the number of fins increases. In contrast, the increase in the fin volume meant a decrease in the amount of energy stored and released, due to the reduction in the PCM quantity contained in the heat exchanger. Fan et al. [16] studied, both numerically and experimentally, the melting of a PCM inside a spherical capsule for thermal energy storage applications. The heat transfer was enhanced by introducing a thin fin inside the capsule. The presence of the fin increased the heat transferred by conduction and yielded the activation of natural convective cells, with consequent improvement on the thermal energy storage performance. Biwole et al. [17] numerically studied the melting of a PCM in a rectangular enclosure exposed to a constant heat flux, with the aim to determine the effects on the heat transfer of the number, dimension and position of metal fins. Their results proved that, either increasing the number of fins, or using longer and thinner fins, accelerates the sensible and latent storage of energy in the PCM. De Césaro Oliveski et al. [18] analyzed the lauric acid melting process in a finned rectangular cavity, changing the fin aspect ratio while keeping the PCM mass and the total fin area constant. For all the cases tested, with an increase in the fin length, a reduction of the PCM melting time was observed. Bouzennada et al. [19] presented a numerical study on the melting of a PCM in a rectangular capsule with a mid-separating fin and different inclination angles. The authors proved that the melting and storing energy rate increases by varying the capsule's

inclination angle from 90° to 0° and that the inclusion of the fin decreases the melting time up to more than 20%.

In this paper, we study the heat exchanges within a PCM inserted in a rectangular enclosure which is bottom heated. Fins are added while maintaining the enclosure area constant, assuming that the space allocated to this heat exchanger is constrained. We question the melting of PCM enhanced by fins on a fundamental level and examine the impact of the different heat transfer mechanisms – conduction and convection – on the melting behavior. A theoretical approach, based on scale analysis, allows to predict the evolution in time of the melt layer with or without fins. A numerical model is dedicated to informing the dynamic aspects as a function of the spacing between fins.

2. Analysis

We consider a rectangular enclosure $L \times H$, where the horizontal dimension $L \gg H$.

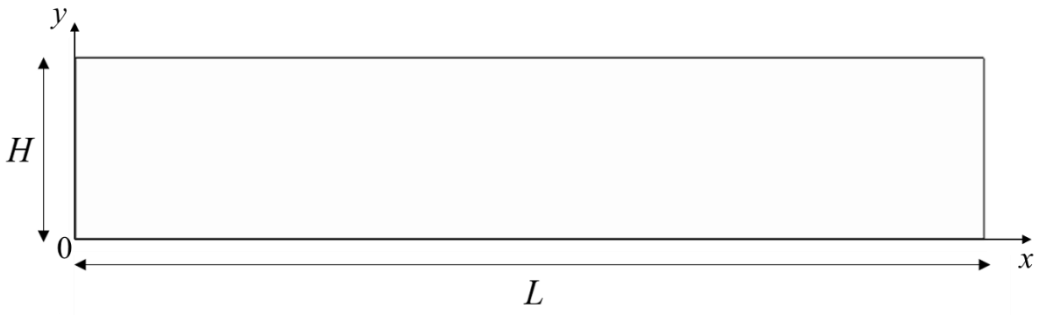

Figure 1: Rectangular enclosure.

The enclosure is filled with PCM (Phase Change Material). It is bottom heated at constant temperature T_H, while the top is adiabatic, together with the vertical walls. Assume the initial temperature of the domain is T_m, the melting temperature of the PCM. While the bottom of the enclosure is brought to $T_H > T_m$, the PCM starts melting first by conduction, then by convection.

The melt layer is $\delta(t)$ and the temperature difference between T_H and T_m is ΔT. An energy balance at the liquid/solid interface of the PCM gives

$$\rho L_f \frac{d\delta}{dt} \sim k \frac{\Delta T}{\delta} \tag{1}$$

where ρ is the PCM density, L_f is the PCM latent heat of fusion, t is time and k is the PCM thermal conductivity. We assume that the density remains constant regardless of the liquid or solid state. Equation (1) allows to obtain the way the conductive liquid layer progresses upward in time.

$$\delta \sim \left(\frac{k\Delta T}{\rho L_f} \right)^{1/2} t^{1/2} \tag{2}$$

Introducing the Stefan number ($Ste = c_p \Delta T / L_f$, where c_p is the heat capacity at constant pressure) and the Fourier number ($Fo = \alpha t / H^2$, where α is the thermal diffusivity), Eq. (2) can also be expressed as

$$\delta / H \sim \left(Ste\, Fo \right)^{1/2} \tag{3}$$

At some point, the purely conductive transport of heat from the bottom of the enclosure to the material is not enough. Convection becomes more efficient, leading to the development of counterrotating convection cells famously known as Rayleigh–Bénard cells [20]-[21]. The change in heat transfer regime is captured by the value of the Rayleigh number based on the melt layer thickness δ, $Ra_\delta = g \beta \Delta T \delta^3 / (\nu \alpha)$, where g is the gravitational acceleration, β is the coefficient of thermal expansion and ν is the kinematic viscosity. Transition between conduction-driven melting and convection-driven melting occurs when $Ra_\delta \cong 10^3$ [22]. In such case, the Nusselt number is given by [23]

$$Nu_\delta = 0.069 Ra_\delta^{1/3} \mathrm{Pr}^{0.074} \tag{4}$$

For a Prandtl number much greater than 1, Eq. (4) can be replaced by

$$Nu_\delta \sim \frac{1}{10} Ra_\delta^{1/3} \tag{5}$$

In the convection regime, the energy balance at the interface between liquid and solid reads

$$\rho L_f \frac{d\delta}{dt} \sim \frac{k\Delta T}{\delta} Nu_\delta \tag{6}$$

because, by definition, the Nusselt number and the heat flux are related by $Nu_\delta = q''\,\delta / (\Delta T\, k)$. Equation (6) clearly shows the augmentation of heat transfer due to convection. Combining Eqs. (5) and (6) together, we obtain the relationship between the melt layer thickness δ and time

$$\delta \sim \frac{1}{10} \frac{k\Delta T}{\rho L_f} \left(\frac{g\beta\Delta T}{\nu\alpha} \right)^{1/3} t \tag{7}$$

or

$$\delta / H \sim \frac{1}{10} Ra_H^{1/3}\, Ste\, Fo \tag{8}$$

Plotted in Figure 2 are Eqs. (2) and (7).

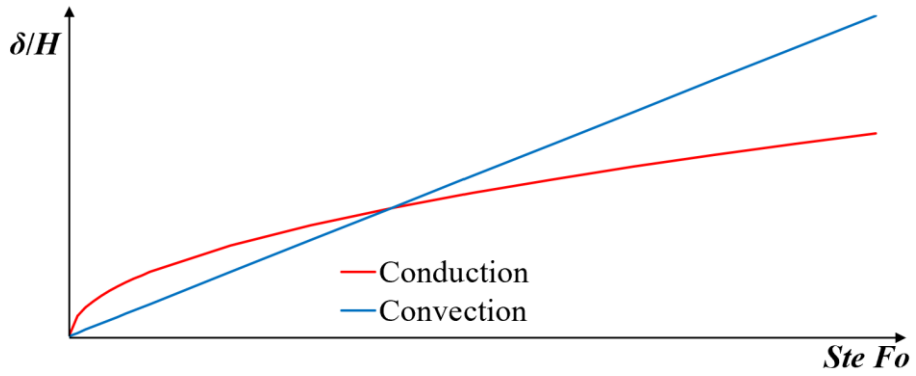

Figure 2: Conduction and convection melt layer as a function of time (non-dimensional terms).

When melting starts, conduction heat transfer is preferred because heat is transferred faster than by convection. In time, convection is more effective and becomes the chosen mode of heat transport. The transition between the two can be estimated by equating Eqs. (2) and (7), leading to

$$t_{trans} \sim 100\left(\frac{k\Delta T}{\rho L_f}\right)^{-1}\left(\frac{g\beta\Delta T}{\nu\alpha}\right)^{-2/3} \tag{9}$$

and

$$\delta_{trans} \sim 10\left(\frac{g\beta\Delta T}{\nu\alpha}\right)^{-1/3} \tag{10}$$

which brings $Ra_\delta \cong 10^3$ as transition between conduction regime and convection regime. Even though convection accelerates the melting of the PCM through the development of Rayleigh-Bénard cells, it may not be enough, calling for more "help". One way to improve melting is to add high conductivity inserts such as metallic fins.

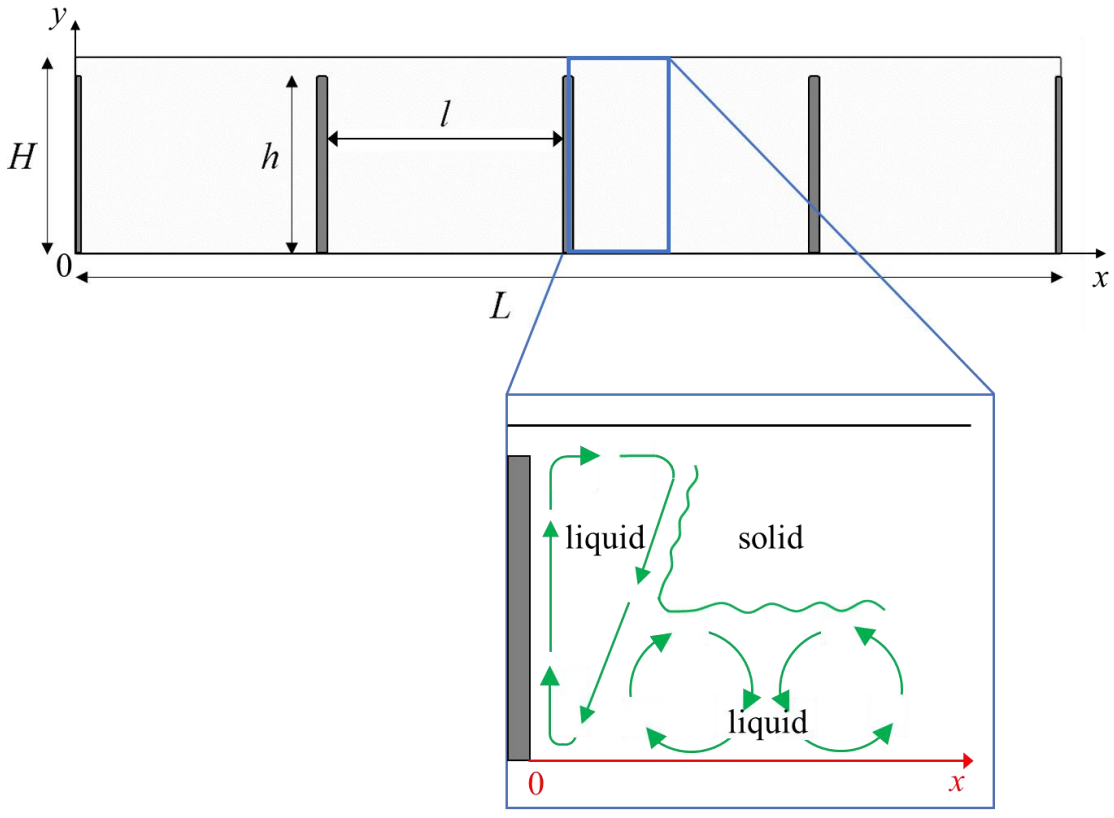

Figure 3: Rectangular enclosure with fins.

As shown in Figure 3, the fins are inserted from the bottom of the enclosure. Their height h is smaller than H because the point is not to convey heat from the enclosure bottom to its top, but to store energy by melting the entire volume of PCM. The spacing between the inserts is l.

Assume that the thermal conductivity of the inserts is high enough to consider that their temperature is uniform and identical to the bottom temperature T_H. Assume also that the melt layer in the bottom is in the convection regime, therefore $\delta(t)$ obeys Eq. (7). Consider the domain delineated by $H \times l/2$. The fin we see in this domain behaves like a hot wall at temperature T_H in contact with a PCM at T_m.

Heat transfer from the fin to the PCM is initially by conduction, then convection. Classically, when considering the heat exchanges between a vertical warm wall and a PCM at a lower temperature, the bottom part of the wall is submitted to conduction while the upper section is dominated by natural convection. Here the case is different because the PCM melts simultaneously from the bottom and from the vertical fin. Therefore, convection is the dominant mechanism between the fin and the PCM, and the upward boundary layer along the fin starts developing from the bottom of the enclosure (see Figure 3).

In the upper zone of the enclosure, the convective flow melts the PCM located between the height of the fin and the height of the enclosure, and expands horizontally moving the melting front away from the fin. The convective flow sinks into the liquid pool, generating a circulation loop upward along the fin, horizontally along the enclosure top wall, and downward along the inclined interface with the solid phase.

The temperature difference across the upward boundary layer is $\Delta T / 2$, and the temperature difference across the downward boundary layer is $\Delta T / 2$. Indeed, as detailed in [24], when the Rayleigh–Bénard cells turns, an excess temperature of order of magnitude $\Delta T / 2$ exists between

the cell and the average value of the temperature of the liquid layer. Recalling that the Prandtl number is greater than 1, the boundary layer thickness δ_* is of order $H\,Ra_{H*}^{-1/4}$, where the Rayleigh number Ra_{H*} is based on $\Delta T/2$. Note that we consider the height of the enclosure, rather than the height of the fin as the heat flow is conveyed all the way up to the top of the cavity. Next, we write the energy conservation at the interface between the downward boundary layer in the liquid phase and the solid phase. The heat flux through the boundary layer is given by $k\frac{\Delta T/2}{\delta_*}$. Combining it with the order of magnitude of δ_*, and using the definition of Ra_{H*}, we obtain

$$\frac{k\Delta T}{2H}\left(\frac{g\,\beta\,\Delta T\,H^3}{2\nu\,\alpha}\right)^{1/4} \sim \rho L_f \frac{dx}{dt} \tag{11}$$

where x is the horizontal distance from the fin.

The thickness of the melt layer that spreads horizontally from the fin along the ceiling of the enclosure is therefore

$$x/H \sim \frac{1}{2^{5/4}} Ra_H^{1/4} Ste\,Fo \tag{12}$$

The ratio between the horizontal melt thickness and the one spreading vertically from the bottom of the enclosure is given by dividing Eq. (12) by Eq. (8). In an order of magnitude sense, we have

$$\frac{x}{\delta} \sim \frac{5}{2^{1/4}} Ra_H^{-1/12} \tag{13}$$

3. Model

3.1 Geometry and materials

A rectangular enclosure with dimensions L = 0.1 m and H = 0.02 m was considered for the numerical study. Different cases were analyzed: either the enclosure contains only the PCM (see

Figure 1), or it includes also a certain number of fins, inserted from the bottom and spaced within the enclosure (see, e.g., Figure 3, representing the case with 5 fins). The fins width and height are 0.001 m and 0.018 m, respectively. It is worth mentioning that the two lateral fins on the vertical walls are half as thick as the others, in order to reduce the edge effects (see Figure 3).

The PCM is octadecane, which thermophysical properties are reported in Table 1 [25]. The fins are made of aluminum (k_f = 237 W/(m K), ρ_f = 2,700 kg/m^3, c_{pf} = 897 J/(kg K)). As indicated in Table 1, the PCM starts melting at a temperature T_m equal to 303 K, while the melting range is ΔT_m = 1 K. It should be noted that different properties for octadecane can be found in the literature [26]-[31]. We have selected Ref. [25], which is a reference in the field, but any change on a property value would not modify the findings of the paper.

Table 1: PCM (octadecane) thermophysical properties [25].

Phase change temperature range, T [K]	303-304
Latent heat of fusion, L_f [J/kg]	125,000
Thermal conductivity, k [W/(m K)]	0.2
Density, ρ [kg/m^3]	800
Specific heat capacity at constant pressure, c_p [J/(kg K)]	1,250
Dynamic viscosity, μ [Pa s]	0.008
Thermal expansion coefficient, β [K^{-1}]	0.002

3.2 Governing equations

In order to study the time-dependent melting of the PCM confined in the rectangular enclosure, the following assumptions are made: i) the PCM in liquid phase is incompressible and the flow

laminar following the Boussinesq approximation; ii) both PCM and metal fins are isotropic; iii) the PCM is bottom heated at constant temperature $T_H > T_m$, while the other boundaries of the enclosure are kept adiabatic as mentioned in Section 2; iv) initially, the enclosure is filled with PCM in solid phase: the initial temperature of the whole domain is uniform and equal to the melting temperature T_m.

The governing equations are the mass, momentum and energy conservation:

$$\nabla \bullet \vec{u} = 0 \tag{14}$$

$$\rho \frac{\partial \vec{u}}{\partial t} + \rho\left(\vec{u} \bullet \nabla\right)\vec{u} = -\nabla p + \mu \nabla^2 \vec{u} + \rho \vec{g} - \rho \vec{g} \beta \left(T - T_m\right)\theta \tag{15}$$

$$\rho c_p^* \frac{DT}{Dt} = k \nabla^2 T \tag{16}$$

where $\vec{u}$ is the velocity vector, p is pressure, θ is the PCM local liquid fraction and c_p^* is the modified specific heat capacity according to the apparent heat capacity formulation.

In particular, θ is a nondimensional parameter quantifying the percentage of liquid phase contained in the mushy zone of the PCM and is equal to 0 if the temperature is lower than T_m (solid phase), is $(T - T_m)/\Delta T_m$ if temperature is between T_m and $T_m + \Delta T_m$ (mushy region) and is equal to 1 for temperatures higher than $T_m + \Delta T_m$ (liquid phase) [32], [33]. The apparent heat capacity formulation is implemented to model the PCM phase transition process [27], [34]. We assume that the PCM thermal conductivity, density and specific heat capacity are identical between solid and liquid phases. As a consequence, the apparent heat capacity formulation involves the adoption, in the energy conservation equation, of the modified specific heat capacity c_p^* defined as

$$c_p^* = c_p \text{ if } T < T_m \text{ or } T > T_m + \Delta T_m \tag{17}$$

$$c_p^* = c_p + \frac{L_f}{\Delta T_m} \text{ if } T_m < T < T_m + \Delta T_m \tag{18}$$

In the cases with fins within the enclosure, heat is transferred along the aluminum fins thanks to conduction

$$\rho_f c_{pf} \frac{\partial T}{\partial t} = k_f \nabla^2 T \tag{19}$$

The boundary conditions correspond to Eqs. (20) - (22), whereas the initial condition is given by Eqs. (23) – (24).

$$\vec{u}(0,y,t) = \vec{u}(L,y,t) = \vec{u}(x,0,t) = \vec{u}(x,H,t) = 0 \tag{20}$$

$$\left.\frac{\partial T}{\partial x}\right|_{x=0} = \left.\frac{\partial T}{\partial x}\right|_{x=L} = \left.\frac{\partial T}{\partial y}\right|_{y=H} = 0 \tag{21}$$

$$T(x,0,t) = T_H \tag{22}$$

$$\vec{u}(x,\mathrm{y},0) = 0 \tag{23}$$

$$T(x,y,0) = T_m \tag{24}$$

The equations set was solved with a finite element commercial package [35]. The PCM dynamic viscosity μ was implemented as a smoothed, continuous, second derivative step function, centered around ($T_m + \Delta T_m/2$) and with values going from 0.008 Pa s in the liquid phase (temperatures above the melting range) to a fictitious value of 10^8 Pa s in the solid phase (temperatures below the melting range).

3.3 Grid independence tests

The 2D computational domain was discretized through an unstructured triangular mesh, optimized for laminar flow, with finer elements and boundary layer mesh along all the walls. In order to check the mesh independence of the results, three different grid sizes were tested for the

simulations with T_H = 47 °C and 0 or 3 fins. The time-dependent values of the average liquid fraction over the entire domain were compared for the different grid sizes as shown in Table 2. Due to the low values of maximum absolute error and root mean square deviation, in terms of average liquid fraction, of Mesh 2 with respect to Mesh 3 (see Table 2), Mesh 2 was considered sufficient.

All simulations were performed selecting a relative tolerance of 0.01 and an absolute tolerance factor equal to 0.1, with automatic computational time step. Results are recorded every second. The time required to run a simulation of 1,500 s is about 2 h on a PC with Intel Core i7-6700K 4.0 GHz, RAM 64 GB.

Table 2: Grid independence tests: maximum absolute error and root mean square deviation (RMSD) in terms of average liquid fraction.

	0 fins			3 fins		
Grid	Number of elements	Max absolute error	RMSD	Number of elements	Max absolute error	RMSD
Mesh 1	6,092	0.0498	0.0383	7,559	0.0390	0.0276
Mesh 2	11,294	0.0152	0.0100	13,068	0.0074	0.0045
Mesh 3	26,012	-	-	31,282	-	-

3.4 Model validation

The numerical model was validated using both the published results from Guo et al. [5] and from Biwole et al [17]. In the first paper the authors numerically studied the melting process of gallium in a square cavity heated from the bottom. The bottom surface of the cavity was heated at constant temperature (higher than the melting temperature), while the other surfaces were adiabatic. The case with *Ste* = 0.148 and $Ra_H = 7.5 \times 10^5$ (corresponding to a square cavity with side 0.087 m) was selected to compare the results with the ones of this work. The average liquid fraction $\bar{\theta}$ is reported in Figure 4 as a function of the dimensionless time *Ste Fo*. A very good agreement

between our numerical results and [5] can be noticed; the maximum absolute error in the values of $\bar{\theta}$ is 0.0214 and the root mean square deviation is 0.0052.

Biwole et al [17] numerically simulated the melting of octadecane in a 2D square cavity of height 0.1 m, heated from the left. In particular, the left vertical surface was heated at a constant temperature higher than the melting temperature, the right vertical surface was kept at a constant temperature equal to the melting temperature and the horizontal walls were adiabatic. Also in this case, an optimal agreement between our results and [17] is obtained, as can be noticed in Figure 5, where the average liquid fraction $\bar{\theta}$ is plotted as a function of the dimensionless time *Ste Fo*. The maximum absolute error in the values of $\bar{\theta}$ is 0.0078 and the root mean square deviation is 0.0043. The good agreement with the results of both Guo et al. [5] and Biwole et al [17] allows to conclude that our model is validated.

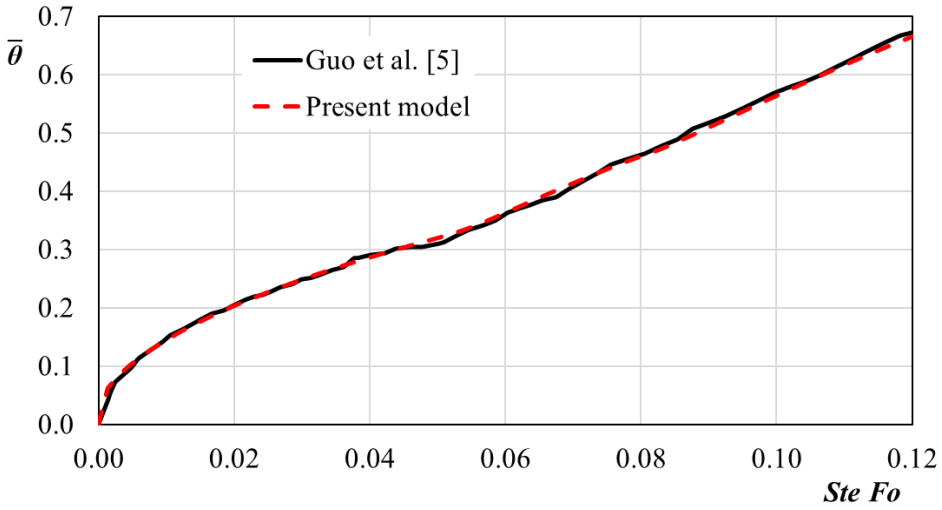

Figure 4: Average liquid fraction of gallium versus dimensionless time, for *Ste* = 0.148 and $Ra_H = 7.5 \times 10^5$, results by Guo et al. [5] and by the present model.

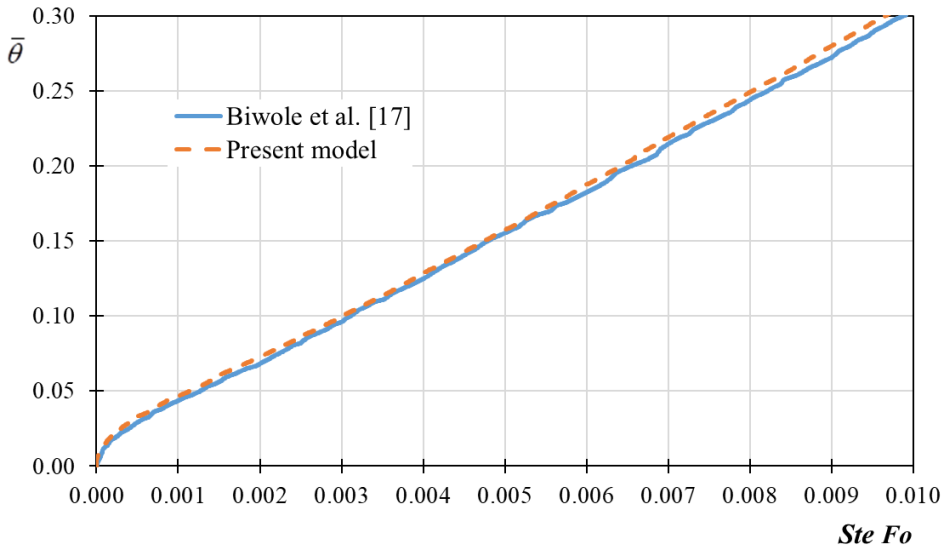

Figure 5: Average liquid fraction of octadecane versus dimensionless time, results by Biwole et al [17] and by the present model.

4 Results

4.1 No fins

We show in Figure 6 the time sequence of the PCM melting in the absence of fins in the cavity for $\Delta T = T_H - T_m = 17$ °C. The Rayleigh number is $Ra_H = 1.35 \times 10^6$. As predicted by the analysis in Section 2, melting is a one-dimensional phenomenon driven by conduction at the start of the process. Rayleigh–Bénard convection rolls form when conduction is not efficient enough to convey the heat upward.

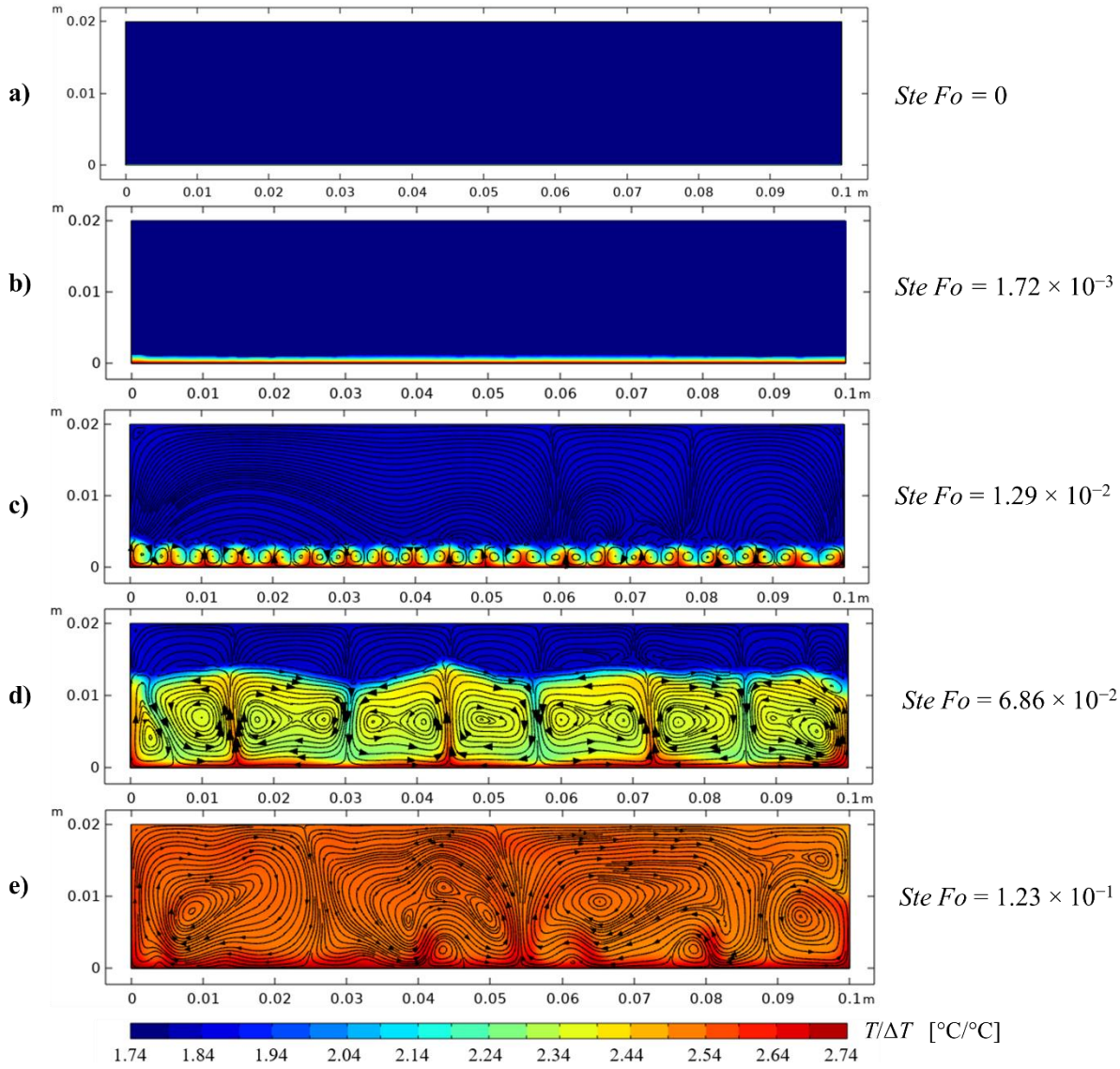

Figure 6: Time sequence of the PCM melting with no fins: (a) initial time, (b) conduction-dominated regime, (c) rolls formation, (d) established rolls, (e) complete melting.

Next, we followed the evolution of the local liquid fraction at mid-distance between the vertical walls of the cavity as a measure of the thickness of the melt layer, δ. δ is the local value of the liquid fraction θ when $\theta = 0.5$ to represent the mushy zone. Figure 7 gives the non-dimensional melt layer thickness δ/H as a function of dimensionless time *Ste Fo*. The evolution of the melt

layer is initially proportional to the square root of time, before becoming linear in time. This behavior is exactly what was anticipated previously by Eqs. (2) and (7).

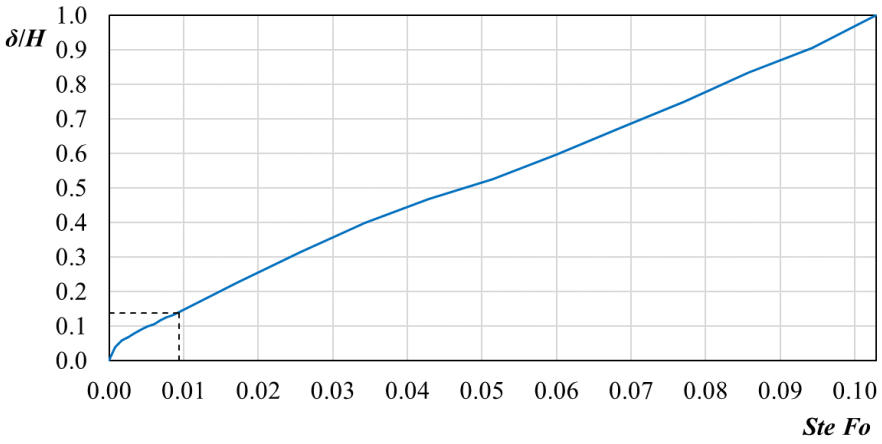

Figure 7: Non-dimensional melt layer thickness as a function of dimensionless time; numerical results with no fins.

Note the inflexion on the curve, which indicates the transition between the conduction regime of melting to the convection-dominated regime. Transition occurs at $Ste\ Fo = 9.35 \times 10^{-3}$ for a melt thickness of $\delta/H = 1.37 \times 10^{-1}$. The theoretical analysis (Eq. (10)) predicted that the transition would occur for a non-dimensional melt layer thickness of 0.91×10^{-1}, and the corresponding non-dimensional time would be 8.20×10^{-3}.

4.2 Addition of fins

As mentioned in the introduction, the addition of fins is made at constant enclosure. The share of PCM compared to the initial configuration without fins is given in Table 3.

We show in Figure 8 the average melting fraction evolution as a function of the dimensionless time *Ste Fo*. The spacings investigated are shown in Table 3.

Table 3: Fins spacing l, aspect ratio H/l and PCM share as functions of the fins number.

Fins number	0	2	3	5	9	17	33
l [mm]	-	99	49	24	11.50	5.25	2.13
H/l	-	0.20	0.41	0.83	1.74	3.81	9.41
PCM area/($L\times H$) [%]	100	99.1	98.2	96.4	92.8	85.6	71.2

The last but one line of Table 3 represents the aspect ratio of the domain generated by two fins and the enclosure height, H/l.

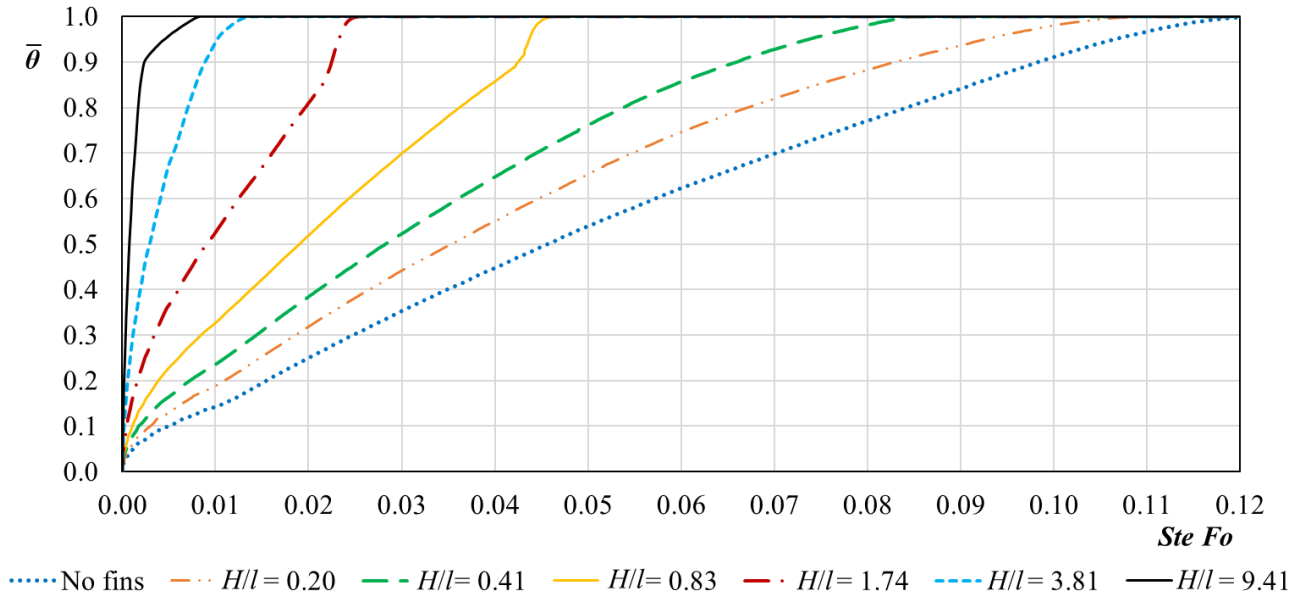

Figure 8: Average melting fraction as a function of dimensionless time, for different H/l.

The presence of fins allows to melt the PCM faster; a result that needs to be weighted by the fact that the total PCM volume decreases with the number of fins added. When the PCM is almost entirely melted, the slope of the average melt fraction changes with either an increase, or a decrease.

For a more precise analysis of the heat exchanges, we varied systematically the spacing between fins starting from l = 99 mm (which corresponds to one fin located on each vertical wall of the enclosure) and decreasing to l = 2.13 mm. This allows to distinguish three different domains named large spacing with $H/l \leq 0.38$, intermediary spacing corresponding to $0.38 < H/l \leq 3.08$, and small spacing when $H/l > 3.08$. In the large spacing scenario, the one-dimensional vertical melting described in the no fins case is still valid. It comes in combination with the melting along the fins that adds to the acceleration of the overall propagation of the liquid phase. Note in Figure 9 that the fins are quasi-immediately isothermal.

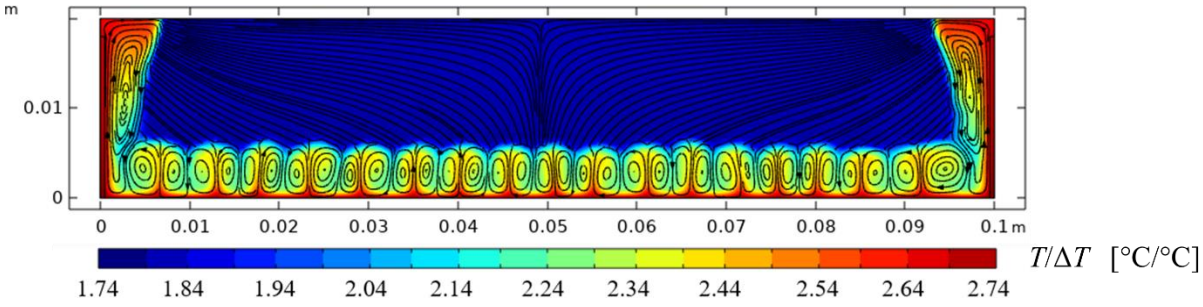

Figure 9: Temperature distribution at *Ste Fo* = 2.57 × 10^{-2}; H/l = 0.20 (2 fins).

As explained in Section 2, a convective cell develops quickly along the fins after a short conduction phase. While the horizontal melting front moves upward, the Rayleigh–Bénard cells become less numerous and grow in size. The cell located in the vicinity of a fin merges with the convective cell along the fin. Then the Rayleigh–Bénard cell immediately adjacent merges also as the vertical and horizontal liquid fronts continue to progress. Finally, a horizontal narrow solid layer remains against the top of the enclosure until it is also melted (see Supplementary material).

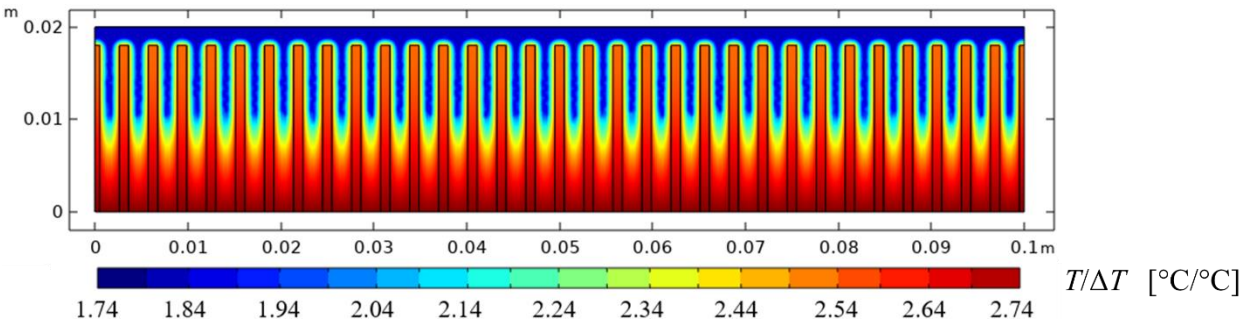

Figure 10: Temperature distribution at *Ste Fo* = 2.14 × 10^{-3}; *H*/*l* = 9.41 (33 fins).

The small spacing case exhibits a totally different behavior (Figure 10). As the fins are brought almost instantaneously to the temperature of the bottom of the enclosure, melting by conduction happens along the fins and the bottom. Melting is so quick that neither Rayleigh–Bénard cells nor convective cells along the fins have time to develop. The volume of PCM contained between fins melts rapidly leading to the sharp slope of the curve in Figure 8. Interestingly the rest of PCM located in the space between the top of the fins and the top of the enclosure needs three times longer to melt, as depicted by the smaller slope of the curve. That layer melts by conduction as the conditions are not met to develop convective cells. Indeed, the thickness of this space is below the criterium for Rayleigh–Bénard cells to be generated (Eq. (3)). A similar behavior is observed when *H*/*l* = 3.81, except that the solid layer above the fins melts faster.

The intermediate spacing scenario corresponds to geometries where the convective channels of liquid PCM that develop horizontally, from the fin along the top of the enclosure, have the time to meet before the entire material changes phase. From Eq. (13), one can anticipate that when $x \sim l/2$, $\delta \sim 0.4\, l$, with the numerical values used in the model, as $x/\delta \sim 1.3$.

We plot in Figure 11 the evolution of *x*/*H*, the non-dimensional horizontal layer at the top of the fin, as a function of the non-dimensional time *Ste Fo*, as predicted by Eq. (12) and as measured from the numerical results, when *H*/*l* = 0.83.

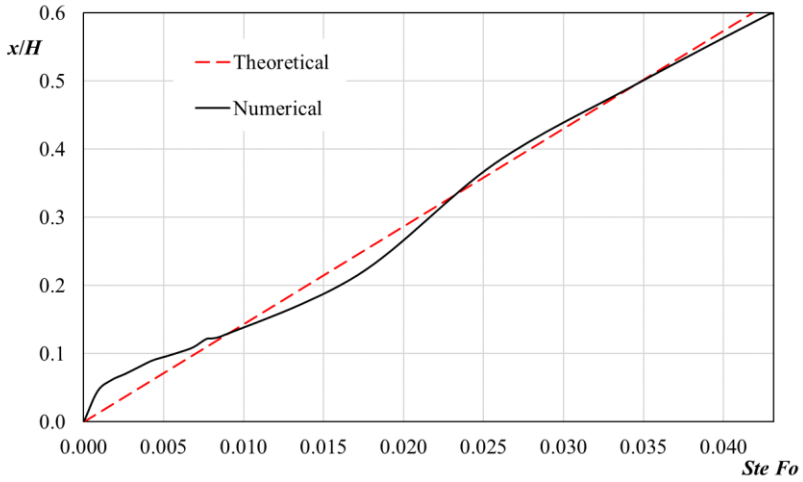

Figure 11: Non-dimensional horizontal layer at the top of the fin as a function of dimensionless time; theoretical vs numerical results with H/l = 0.83 (5 fins).

Note the good agreement between the two results beyond $Ste\ Fo = 8.58 \times 10^{-3}$. Below this threshold the results do not match. Indeed, the theoretical analysis is based on the existence of the two boundary layers in the convective cell, one moving upward along the fin and the other one sinking along the melting front.

When H/l varies between 0.38 and 3.08, while the PCM melts, comes a time when the liquid layers at the top of the enclosure meet. This time is different from one aspect ratio to the other. We show in Figure 12 the example of H/l = 0.83 which corresponds to five fins as described in Table 3. In Figure 12, instead of showing the entire enclosure, we chose to show only a portion held between two fins and the top and bottom boundaries.

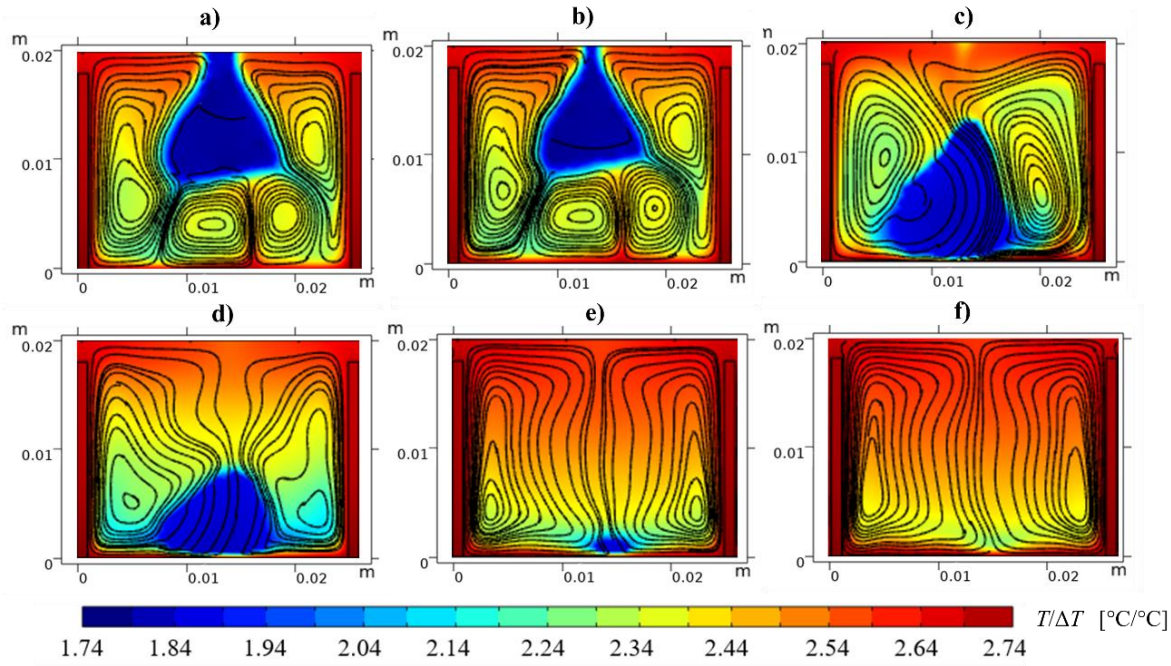

Figure 12: Time sequence of the solid drop formation and sink between two fins (H/l = 0.83): (a) *Ste Fo* = 4.12×10^{-2}, (b) *Ste Fo* = 4.30×10^{-2}, (c) *Ste Fo* = 4.32×10^{-2}, (d) *Ste Fo* = 4.37×10^{-2}, (e) *Ste Fo* = 4.57×10^{-2}, (f) *Ste Fo* = 4.61×10^{-2}. We present here only a portion of the enclosure delimited by two fins and the top and bottom boundaries.

As can be seen in the figure, in this situation a solid domain, shaped as a drop, is trapped between liquid domains: the two liquid loops generated by the PCM melting in the vicinity of the fins, wide at the top of the enclosure and narrower towards the bottom, and the horizontal liquid layer formed by the Rayleigh–Bénard cells. As time increases, the solid drop is dragged towards the bottom of the enclosure. This phenomenon is made possible because the convective loops that exist along each fin have a downward liquid flow at their interface with the solid PCM. The generated shear forces pull the solid drop down into the bottom liquid pool. The latter is viscous enough to let the solid drop sink, moving away the Rayleigh–Bénard cells. Now in direct contact with the heated bottom, the remaining solid melts entirely.

The occurrence of the solid drop is caught in Figure 8, with the sharp change in the slope of the average melting fraction. Unlike in the case of small spacings, the change in slope is positive as the fall of the solid drop accelerates the melting of the volume of PCM that was not liquid yet.

5 Conclusion

The paper offers a theoretical approach of the melting of PCM in a bottom-heated enclosure, with or without metallic fins, relying on scale analysis. The proposed approach is validated by numerical experiments.

The main conclusions that can be drawn are:

- The melt layer varies first with the square root of time (conduction melting), then linearly with time (convection melting), because convection becomes in time more effective than conduction.
- When vertical fins are added to the enclosure, a vertical convective loop of liquid PCM is generated along the fins. Its melting front propagates horizontally, away from the fin, and the distance from the fin is larger at the top of the enclosure.
- The horizontal propagation of the melt layer is ~30% bigger than the vertical propagation of the bottom liquid layer, for the parameters of the study (geometry and PCM properties).
- The work identifies the existence of three very different thermal behaviors: a Rayleigh–Bénard cells dominated regime for large fins spacings, a conduction dominated melting regime for small fins spacings, and a solid drop generated regime for the intermediary spacing configurations.
- The solid drops are created when the horizontal convective liquid PCM channels emanating from the fins become in contact along the top of the cavity. The downward flows of liquid

PCM on the two sides drag the solid drop down, helping it to sink into the liquid bottom layer where it ends melting.

Acknowledgments

Giulia Martino's Ph.D. scholarship is funded by the MIUR (Italian Minister for University and Research) and "PON Research and Innovation 2014-2020 - Education and Research for recovery REACT-EU", Action IV.5.

This work was initiated during Sylvie Lorente's stay at the University of Bologna as Senior Visiting Fellow during the summer of 2022.

Supplementary materials

Supplementary materials (movies) associated with this article can be found in the online version.

REFERENCES

[1] S. Lorente, A. Bejan, J.L. Niu, Phase change heat storage in an enclosure with vertical pipe in the center, International Journal of Heat and Mass Transfer, 72, 329–335, 2014.

[2] S. Lorente, A. Bejan, J.L. Niu, Constructal design of latent thermal energy storage with vertical spiral heaters, International Journal of Heat and Mass Transfer, 81, 283–288, 2015.

[3] M. Parsazadeh, X. Duan, Numerical and Experimental Investigation of Phase Change Heat Transfer in the Presence of Rayleigh–Benard Convection, ASME J. Heat Transfer, 142, 062401, 2020.

[4] M. Parsazadeh, M. Malik, X. Duan, A. McDonald, Numerical study on melting of phase change material in an enclosure subject to Neumann boundary condition in the presence of

Rayleigh-Bénard convection, International Journal of Heat and Mass Transfer, 171, 121103, 2021.

[5] W. Guo, R. Zhao, Y. Liu, D. Huang, Semi-theoretical correlations of melting process driven by Rayleigh–Bénard convection suitable for low melting point metal, Case Studies in Thermal Engineering, 28, 101511, 2021.

[6] O. Satbhai, S. Roy, Criteria for the onset of convection in the phase-change Rayleigh–Bénard system with moving melting-boundary, Physics of Fluids, 32, 064107, 2020.

[7] S. Xie, W. Wu, Effect of aspect ratio on PCM melting behavior in a square cavity, International Communications in Heat and Mass Transfer, 143, 106708, 2023.

[8] S. Harish, D. Orejon, Y. Takata, M. Kohno, Thermal conductivity enhancement of lauric acid phase change nanocomposite with graphene nanoplatelets, Applied Thermal Engineering, 80, 205-211, 2015.

[9] L.W. Fan, X. Fang, X. Wang, Y. Zeng, Y.Q. Xiao, Z.T. Yu, X. Xu, Y.C. Hu, K.F. Cen, Effects of various carbon nanofillers on the thermal conductivity and energy storage properties of paraffin-based nanocomposite phase change materials, Applied Energy, 110, 163-172, 2013.

[10] J.M. Khodadadi, S.F. Hosseinizadeh, Nanoparticle-enhanced phase change materials (NEPCM) with great potential for improved thermal energy storage, International Communications in Heat and Mass Transfer, 34, 534–54, 2007.

[11] X. Xiao, P. Zhang, M. Li, Effective thermal conductivity of open-cell metal foams impregnated with pure paraffin for latent heat storage, International Journal of Thermal Sciences, 81, 94-105, 2014.

[12] X. Huang, Y. Lin, G. Alva, G. Fang, Thermal properties and thermal conductivity enhancement of composite phase change materials using myristyl alcohol/metal foam for solar thermal storage, Solar Energy Materials and Solar Cells, 170, 68-76, 2017.

[13] X. Hu, F. Zhu, X. Gong, Experimental and numerical study on the thermal behavior of phase change material infiltrated in low porosity metal foam, Journal of Energy Storage, 26, 101005, 2019.

[14] W. Cui, T. Si, X. Li, X. Li, L. Lu, T. Ma, Q. Wang, Heat transfer enhancement of phase change materials embedded with metal foam for thermal energy storage: A review, Renewable and Sustainable Energy Reviews, 169, 112912, 2022.

[15] A. Shukla, K. Kant, P.H. Biwole, R. Pitchumani, A. Sharma, Melting and solidification of a phase change material with constructal tree-shaped fins for thermal energy storage, Journal of Energy Storage, 53, 105158, 2022.

[16] L.W. Fan, Z.Q. Zhu, S.L. Xiao, M.J. Liu, H. Lu, Y. Zen, Z.T. Yu, K.F. Cen, An experimental and numerical investigation of constrained melting heat transfer of a phase

change material in a circumferentially finned spherical capsule for thermal energy storage, Applied Thermal Engineering, 100, 1063–1075, 2016.

[17] P.H. Biwole, D. Groulx, F. Souayfane, T. Chiu, Influence of fin size and distribution on solid-liquid phase change in a rectangular enclosure, International Journal of Thermal Sciences, 124, 433-466, 2018.

[18] R.D.C Oliveski, F. Becker, L.A.O Rocha, C. Biserni, G.E.S. Eberhardt, Design of fin structures for phase change material (PCM) melting process in rectangular cavities, Journal of Energy Storage, 35, 102337, 2021.

[19] T. Bouzennada, F. Mechighel, T. Ismail, L. Kolsi, K. Ghachem, Heat transfer and fluid flow in a PCM-filled enclosure: effect of inclination angle and mid-separation fin, International Communications in Heat and Mass Transfer, 124, 105280, 2021.

[20] A. Bejan, Convection Heat Transfer, John Wiley & Sons, 2013.

[21] A.V. Getling, Rayleigh-Bénard Convection: Structures and Dynamics, World Scientific Publishing, 1998.

[22] F.H. Busse, Non-linear properties of thermal convection, Reports on Progress in Physics, 41, 1929-67, 1978.

[23] S. Globe, D. Dropkin, Natural-convection heat transfer in liquids confined by two horizontal plates and heated from below, ASME Journal of Heat Transfer, 81, 24-24, 1959.

[24] R.A. Nelson, Jr., A. Bejan, Constructal Optimization of Internal Flow Geometry in Convection, ASME J. Heat Transfer, 120, 357-364, 1998.

[25] O. Bertrand, B. Binet, H. Combeau, S. Couturier, Y. Delannoy, D. Gobin, M. Lacroix, P. Le Quere, M. Medale, J. Mencinger, H. Sadat, G. Vieira, Melting driven by natural convection - A comparison exercise: first results, International Journal of Thermal Sciences, 38, 5-26, 1999.

[26] R.E. Murray, D. Groulx, Modeling Convection during Melting of a Phase Change Material, Proceedings of the COMSOL Conference, Boston, 13-15 October 2011.

[27] S. Ziaei, S. Lorente, A. Bejan, Constructal design for convection melting of a phase change body, International Journal of Heat and Mass Transfer, 99, 762–769, 2016.

[28] F.L. Tan, S.F. Hosseinizadeh, J.M. Khodadadi, L. Fan, Experimental and computational study of constrained melting of phase change materials (PCM) inside a spherical capsule, International Journal of Heat and Mass Transfer, 52, 3464–3472, 2009.

[29] S. Madruga, J. Curbelo, Dynamic of plumes and scaling during the melting of a Phase Change Material heated from below, International Journal of Heat and Mass Transfer, 126, 206–220, 2018.

[30] N.H. Boukani, A. Dadvand, A.J. Chamkha, Melting of a Nano-enhanced Phase Change Material (NePCM) in partially-filled horizontal elliptical capsules with different aspect ratios, International Journal of Mechanical Sciences, 149, 164-177, 2018.

[31] M. Faden, S. Höhlein, J. Wanner, A. König-Haagen, D. Brüggemann, Review of thermophysical property data of octadecane for phase-change studies, Materials, 12, 2974, 2019.

[32] N. Bianco, A. Fragnito, M. Iasiello, G.M. Mauro, L. Mongibello, Multi-objective optimization of a phase change material-based shell-and-tube heat exchanger for cold thermal energy storage: experiments and numerical modeling, Applied Thermal Engineering, 215, 119047, 2022.

[33] M. Iasiello, M. Mameli, S. Filippeschi, N. Bianco, Metal foam/PCM melting evolution analysis: Orientation and morphology effects, Applied Thermal Engineering, 187, 116572, 2021.

[34] C. Naldi, M. Dongellini, G.L. Morini, The evaluation of the effective thermal conductivity of metal-foam loaded phase change materials, Journal of Energy Storage, 51, 104450, 2022.

[35] COMSOL Multiphysics, https://www.comsol.com/ (last accessed on June 21, 2023).